Creep behavior of Ti-6Al-4V alloy specimens produced by Electron Beam Melting

P. Aliprandi, F. Giudice, E. Guglielmino, G. La Rosa, A. Sili

The development of the so-called additive methods is currently considered of great interest in the manufacturing industry. In particular the Electron Beam Melting (EBM) technique, based on the deposition of individual layers of metal powders which undergo progressively to the passage of an electron beam, is now widely utilized for production of peculiar shapes, both in biomedical and industrial field. In the present work, the mechanical behavior of bulk specimens made of Ti-6Al-4V alloy produced by EBM is investigated, focusing creep behavior in the range 400-600°C which is largely considered for aeronautical applications. Specimens obtained by varying the direction of powder deposition were taken into account, in order to highlight the effects of layers orientation on mechanical properties. The results of creep test were analyzed by means of the Larson Miller parameter, in order to extrapolate creep life at different values of load and temperature.

KEYWORDS: TI-6AL-4V ALLOY – ELECTRON BEAM MELTING (EBM) – CREEP – LARSON MILLER PARAMETER.

INTRODUCTION

The Ti-6Al-4V titanium alloy is characterized by excellent mechanical strength even at high temperature, especially considering also its low density, together with good toughness and corrosion resistance, properties that make it suitable for many applications from spatial to biomedical industry. This alloy, containing 6% of Aluminum (stabilizer of the α phase) and 4% of Vanadium (stabilizer of the β phase), gives rise to a wide range of microstructures with different mechanical properties, according to production process and heat treatment.

The choice of a specific process depends on various factors such as the geometric complexity of the objects, the amount of production and the related costs. Nowadays the additive techniques are quite promising compared to the traditional methods of casting or hot forging, thanks to their ability to obtain artifacts characterized by particular shapes, even very complex, starting from metal powders [1, 2, 3]. Among these techniques, Electron Beam Melting allows to obtain trabecular or bulk products with complex shapes and excellent mechanical properties [4, 5]; moreover, since it operates in vacuum conditions, there are great advantages in the case of metals, such as Titanium, with high affinity for Oxygen [6]; however EBM products are strictly influenced by the process parameters, that result determining for the characteristics of each deposited layer and for the interactions between them, with consequent effects on mechanical properties [7, 8].

This work focuses on the production by EBM of bulk flat specimens made of Ti-6Al-4V alloy and on the study of their tensile and creep behavior, in a temperature range between 400 and 600°C of great interest for applications in aeronautics. These specimens were produced with two different modes of powder deposition, in order to highlight the effects of the direction of layers growth on mechanical properties at room and high temperature. Observations of optical and Electronic Scanning Microscopy (SEM) were carried out on the specimens cross sections after metallographic preparation. The creep test results were analyzed through the Larson Miller parameter, in order to make feasible the extrapolation of creep life at different loads and temperatures.

P. Aliprandi, E. Guglielmino, A. Sili
Dipartimento di Ingegneria -
Università di Messina -
Contrada di Dio, 98166 Messina - Italy

F. Giudice, G. La Rosa
Dipartimento di Ingegneria Civile e Architettura -
Università di Catania -
Via Santa Sofia 64 95123 Catania - Italy

MATERIALS AND EXPERIMENTAL METHODS

The Electron Beam Melting additive technology is based on the use of an electron beam that melts metal powders deposited layer by layer, in order to reproduce three-dimensional models with specific geometries and massive or controlled density cellular structures [9, 10, 11].

Figure 1a shows the main components of an EBM machine [12]. The electron beam generation column comprises the cathode, consisting of a heated tungsten filament, which emits electrons that are accelerated by a potential difference, giving rise to the beam. The shape and deflection of the beam are controlled by magnetic lenses. A first set of lens (astigmatism lens) corrects the shape of the beam, a second set (focus lens) controls its size, the last set (deflection lens) is used to orientate and position the beam.

The build chamber consists of a tank and the powders supply system. The tank contains the process platform (start plane) which constitutes the building plane x-y and can be moved along the vertical axis z. The powder feeding and deposition system consists of two hoppers, a rake that distributes the powder on the building plane and controls the amount of powder distributed and the layer uniformity, in order to avoid uneven thickness that could cause discontinuity in the melt.

The process develops according to some sequential steps [13], starting with the heating of the start plane before the deposition of the first layer of powder, at a temperature defined on the basis of the powder material to be melted. After depositing each layer, the powder bed is preheated by means of a series of non-focused, high-power and high-speed electronic beam passages. The power and the scanning speed are reduced in the subsequent phase of selective fusion, during which the beam is concentrated. After completing the first layer melting, the process platform is lowered by the thickness of a layer to allow the deposition of a new layer of powders to be processed. The sequence is repeated until the whole component is built.

Unlike other fusion additive processes, EBM provides preheating of the powders before the melting phase, which causes a slight sintering, improves the electrical and thermal conductivity and the mechanical stability of the powder bed, and reduces the temperature gradient, avoiding the onset of micro-fractures due to thermal variations [10].

The whole process takes place in a vacuum (10^{-3} Pa) to prevent the air molecules from disturbing the electron beam. During the selective melting phase, a small amount of low pressure inert gas (helium at 10^{-1} Pa) is added to avoid the accumulation of electric charges in the powder, and to guarantee the thermal stability of the process, at the end of which the gas pressure is increased to facilitate cooling [11].

In the proposed work the specimens were made using the Arcam Q10 machine. Figure 1b shows the two different types of specimens produced, with different positioning with respect to the process plane (x-y) and to the building direction (z):

- type A specimens, in which the longitudinal section is coplanar with the process plane, and therefore the layering direction (z axis) is orthogonal to loading direction (x axis);
- type B specimens, in which the cross section is coplanar with the process plane, and therefore the layering direction coincides with loading direction.

In Figure 1c the scanning strategy adopted (pattern of the scanning lines), of the "snake xy" type [14], is schematised: for each layer, the electron beam suitably concentrated to obtain the fusion, impacts on the bed of pre-sintered powders describing a path with alternating parallel lines; between one layer and the next, the direction of the alternating lines is rotated by 90°, in order to cross the path of the previous layer. This type of scanning allows to obtain components whose properties can be considered homogeneous with regards to the two orthogonal directions coinciding with the x-y axes of the process plane.

The main process parameters set for the specimens production are shown in Table 1. They were optimised with the aim to reduce defects, as surface roughness, porosity, unmelted regions and delamination, according to the guideline given in [15].

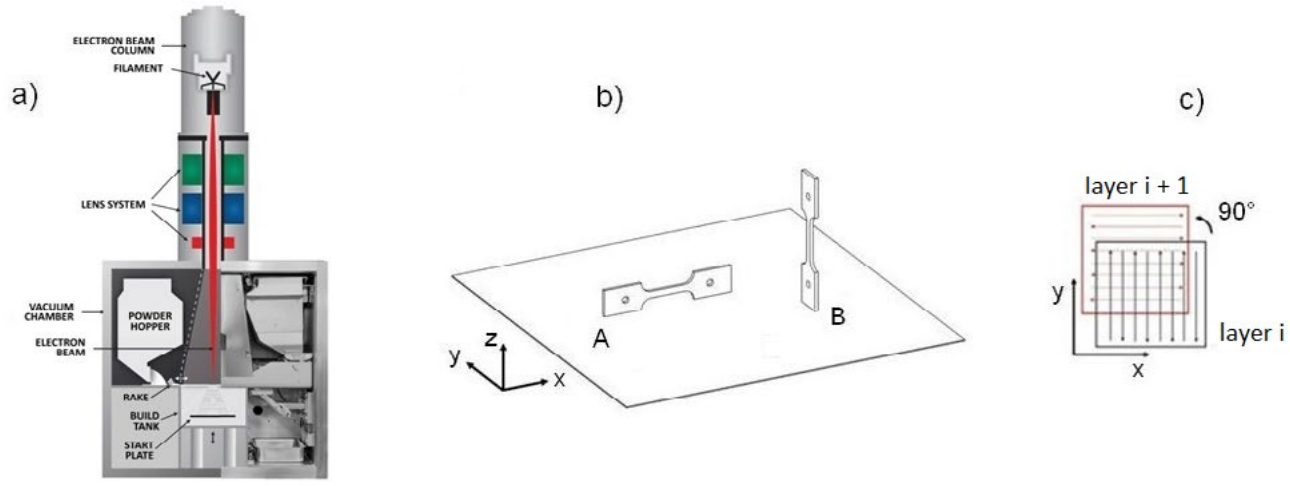

Fig. 1 – EBM process: a) device section [12], b) specimens typology with different position with respect to the process plane, c) pattern of scanning line (snake x-y type) [14].

Tab. 1 – Parameters of the EBM process.

Acceleration voltage	60 kV
Beam current intensity	15 mA
Beam width	200 µm
Scanning speed	4500 mm/s
Line energy	200 J/m
Line offset	100 µm
Layer thickness	50 µm

The tensile and creep specimens were produced by EBM, using as building material Arcam AB powder (grain size between 45 and 100 µm) of the Ti-6Al-4V ELI - Grade 23 alloy, with reduced O, N, C and Fe contents (Table 2). The low content of interstitial elements allows greater ductility and fracture toughness compared to the basic Grade 5 powder.

Tab. 2 – Powder composition and composition range of the alloy Ti-6Al-4V ELI - Grade 23 (weight %).

Al	V	C	Fe	O	N	H	Ti
Composition of the powder used							
6.0	4.0	0.03	0.1	0.1	0.01	<0.003	Bal.
Limits in composition range of the alloy Ti-6Al-4V ELI - Grade 23 (ASTM F136)							
5.5-6.5	3.5-4.5	<0.08	<0.25	<0.13	<0.05	<0.012	Bal.

The composition of the specimens was verified by XRF spectrophotometry, measuring Al content around 5%, lower that the nominal one, attributable to Al volatility at the temperatures reached in the fusion bath, as found by other authors [13].
Geometry and dimensions of the specimens (gage length of 32 mm, width 6 mm and thickness 3 mm) were designed in accordance with ASTM E8 M. The observations by optical and scanning electron microscopy (SEM) was operated on the resistant sections (z-y for specimens A, and x-y for specimens B), prepared according to the usual metallographic methods, and etched for 10 s by the Kroll reagent. Vickers micro-hardness tests were carried out on the same sections. Tensile tests were performed in strain control, with a speed of 2.6×10^{-3} s^{-1}, at room temperature and in the range between 400 and 600 °C. Creep tests were carried out at the same temperatures, by setting the constant load as a fraction of the corresponding yield load, in order to obtain the stationary phase strain rate not higher than 10^{-5} s^{-1}.

RISULTS AND DISCUSSION

Metallographic investigation

The Ti-6Al-4V alloy has different microstructures, according to the thermo-mechanical and/or thermal treatment performed, which can be classified as equiaxed, lamellar or bimodal [16]. The first one consists of a uniform α microstructure, obtained by means of heating below the ß-transus temperature (about 980°C) followed by slow cooling to complete the α grains formation; it shows great ductility and high resistance to fatigue crack initiation [17]. Thermal treatments at temperature higher than the ß-transus temperature lead to fully lamellar α-ß microstructures, classified as "basket weave", which become thinner at the increasing of the cooling rate [18]; in particular water quenching gives rise to the formation of the α' martensitic phase, with an acicular morphology and hardening effects that can be enhanced by successive annealing [19]. The bimodal microstructure, characterized by α grains surrounded by colonies of α-ß lamellas, can be observed with a thermal treating below the ß-transus temperature followed by cooling at sufficiently high rate to avoid the formation of only the α phase [16]; the bimodal microstructure has excellent fatigue properties, because the high resistance to crack initiation of the equiaxed microstructure (greater than the basket weave one where lamellas act as sites for crack nucleation) is balanced with the lamellas ability to delay crack propagation. For this reason the bimodal microstructure shows a very good behavior in high cycle fatigue [20].
In the case of A specimens, where the growth direction (z axis) lies in the micrograph plane (z-y cross section), the deposited powder layers, interspaced of about 50 µm, are well delineated by the boundary of the prior ß grains developed during solidification (figure 2a); the basket weave microstructure took place

during the cooling stage in the form of α-ß colonies, because cooling conditions was not too severe, due to the extension of the deposition plane in the A specimens and to the heating caused by the layers overlapping. Microhardness of the A specimens is about 330 HV.
In the B specimens the growth direction (z axis) is orthogonal to the micrograph plane and microstructure is more narrow, partly recognizable as martensitic acicular (figure 2b). It is due to the faster cooling rate of the layers, which is a consequence of the limited extension of the deposition plane (x-y cross section). Type B specimens show higher microhardness (about 355 HV).

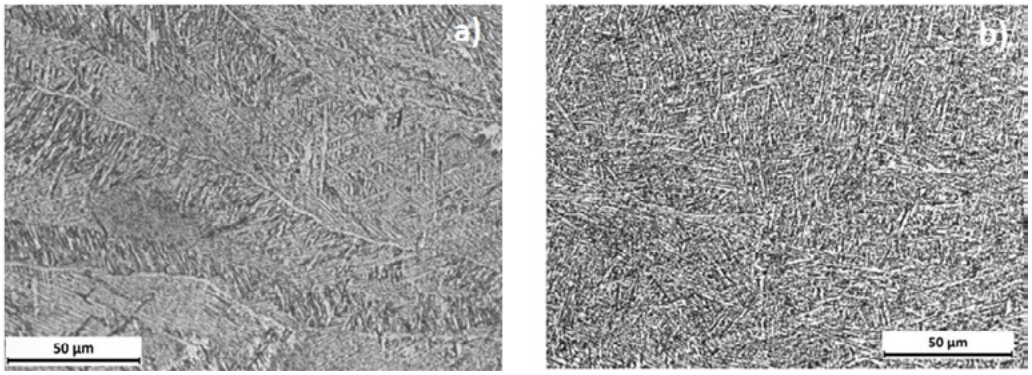

Fig. 2 – Optical micrographs performed on the specimens cross sections: a) type A specimen (z-y plane), b) type B specimen (x-y plane).

Tensile and creep test

The stress-strain curves for the two types of specimens are given in figure 3. The A specimens have greater mechanical strength than the B ones. In both the two case proof stress at room temperature is about 80% of the ultimate strength, elongation is below 10% and necking negligible. At the increasing of test temperature, ductility increases and mechanical strength decreases maintaining in any case appreciable values.
Fracture surfaces have predominantly a ductile appearance, even if some planes of direct separation are easily recognizable close to spherical voids (figure 4a). These voids can be also observed by metallographic investigations on the cross sections (figure 4b), explaining why mechanical strength is lower than that measured on forged specimens of the Ti-6Al-4V alloy with the same basket weave microstructure [20, 21]. Microvoids are common defects in additive manufacturing and those with regular spherical shape can be ascribed to gas trapped between particles during the atomization process of powder, or to pores formation in molten bath by the shielding gas, or to alloy vapors produced during melting [13, 22].
Creep behavior is very sensitive to the test temperature: the strain-time curves in figure 5a show a remarkable increment of the stationary creep rate when temperature changes from 400 to 500°C, indicating high values of the activation energy (calculated around 300 kJ / mol in [23]).
The creep test results are plotted in figure 5b, being σ (Mpa) the test load and LMP = T(C + log t) the Larson Miller Parameter, with T(K) test temperature, t(h) rupture time and C a characteristic constant, assumed equal to 20 according to literature [24]. The A specimens have better creep strength at the two extremes of the Larson Miller diagram, while in the central zone, that refers to testing temperature equal to 500°C, the B specimen shows a greater rupture time than the A one, probably thanks to aging effects as pointed out in [18] for martensitic microstructure.

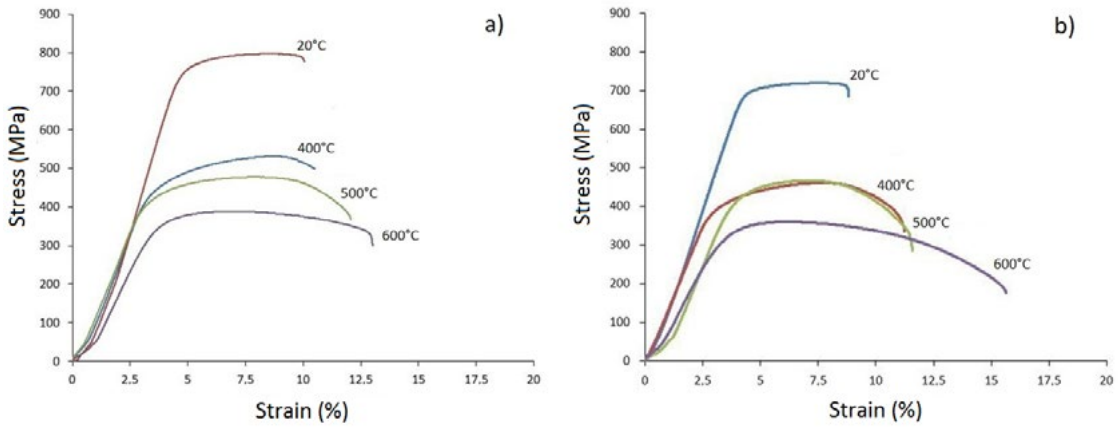

Fig. 3 – Stress-strain curves obtained by tensile test: a) A specimens, b) B specimens.

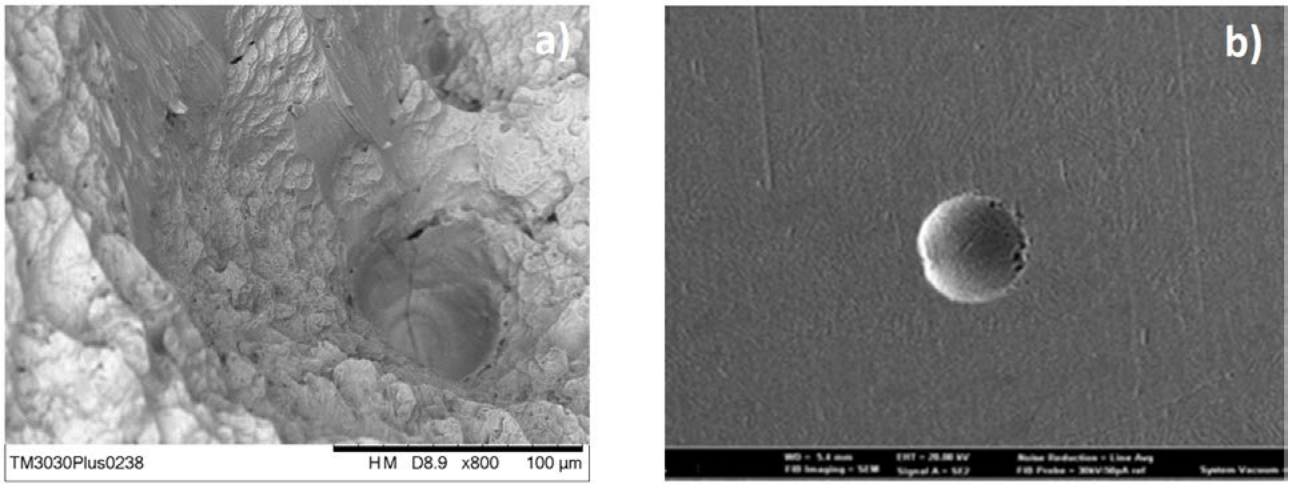

Fig. 4 – SEM micrographs: a) fracture surface at 20°C, b) specimen cross section with a spherical void.

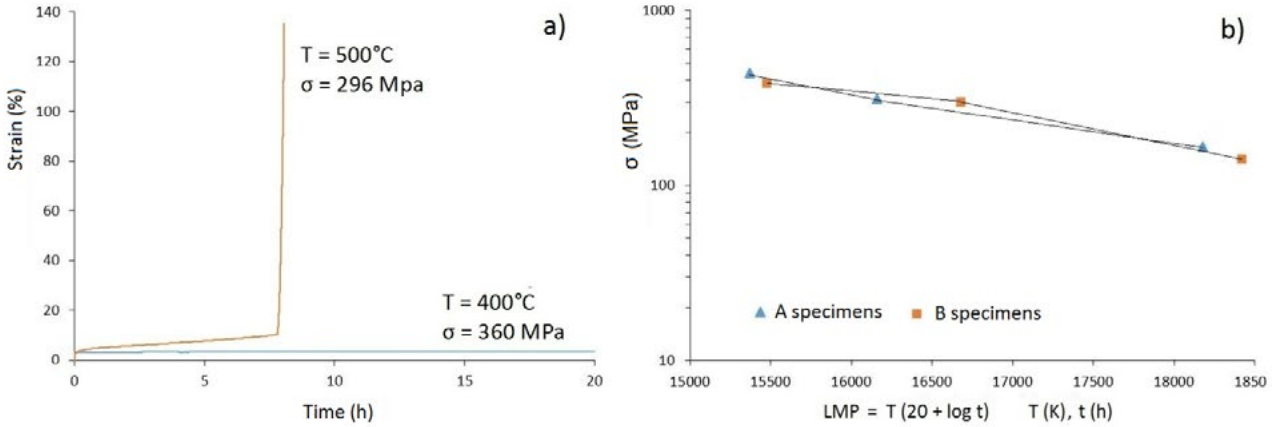

Fig. 5 – Creep test results: a) strain-time curves (specimens A), b) Larson Miller diagram.

CONCLUSIONS

Specimens for tensile and creep tests made of Ti-6Al-4V alloy were produced by means of the EBM additive technique using two different orientations for powder deposition: layers parallel or orthogonal to the tensile test axis, in order to highlight the effect of directionality on mechanical properties. In the first type of specimens, the metallographic investigations on the cross sections show a basket wave microstructure, with elongated grains along the tensile direction; in the second type, grains growth on plane orthogonal to the tensile direction and their microstructure appears finer, in part acicular, as a consequence of more severe cooling conditions. The best tensile properties, both at room temperature and in the range between 400 and 600°C, were measured in the first type of specimens thanks to the microstructure alignment with the tensile direction. With regard to creep behavior, good performances were observed: in the central tract of the Larson Miller diagram the best behavior is shown by the specimen of the second type and it is probably due to ageing effects.

ACKNOWLEDGMENTS

The authors wish to thank the company MT Ortho (Aci S. Antonio CT, Italy) and in particular Eng. Simone Di Bella, to have kindly made the specimens, for providing all the information on the process parameters and for the useful suggestions.

BIBLIOGRAFIA

[1] Frazier, WJ. Metal Additive Manufacturing: A Review. Mater. Eng. Perform. 2014; 23: 1917–1928.

[2] Gibson I, Rosen D, Strucker B. Additive Manufacturing Technologies: 3D Printing, Rapid Prototyping, and Direct Digital Manufacturing, New York: Springer; 2015

[3] Herzog D, Seyda V, Wycisk E, Emmelmann C. Additive manufacturing of metals. Acta Mater. 2016; 117:371–392.

[4] Tan XP, Kok YH, Tan YJ, Descoins M, Mangelinck D, Tor SB, Leong KF, Chua CK. Graded microstructure and mechanical properties of additive manufactured Ti-6Al-4V via electron beam melting. Acta Mater. 2015; 97: 1–16.

[5] Mostafaei A, Toman J, Stevens EL, Hughes ET, Krimer YL, Chmielus M. Microstructural evolution and mechanical properties of differently heat-treated binder jet printed samples from gas-and water-atomized alloy 625 powders. Acta Mater. 2017; 124: 280–289.

[6] Svensson M, Ackelid U. Influence of Interstitial Elements on the Mechanical Properties of Ti-6Al-4V Produced with Electron Beam Melting. Materials Science and Technology Conf. MS&T'11. October 16-20, 2011, Columbus, OH.

[7] Al-Bermani SS, Blackmore ML, Zhang W, Todd I. The origin of microstructural diversity, texture, and mechanical properties in electron beam melted Ti-6Al-4V. Metallurgical and Materials Transactions A, 2010; 41A: 3422-3434.

[8] Morita T, Tsuda C, Nakano T. Influences of scanning speed and short-time heat treatment on fundamental. Materials Science & Engineering, 2017; A 704: 246–251

[9] Milberg J, Sigl M. Electron beam sintering of metal powder, Production Engineering. 2008; 2: 117-122.

[10] Murr LE, Gaytan SM, Ramirez DA, Martinez E, Hernandez J, Amato KN, Shindo PW, Medina FR, Wicker RB. Metal fabrication by additive manufacturing using laser and electron beam melting technologies. Journal of Materials Science & Technology, 2012; 28: 1-14.

[11] Gong X, Anderson T, Chou K. Review on powder-based electron beam additive manufacturing technology. Manufacturing Review, 2014; 1: 1-12.

[12] Arcam AB, www.arcam.com, accessed in May 2018

[13] Gaytan SM, Murr LE, Medina F, Martinez E, Lopez MI, Wicker RB. Advanced metal powder based manufacturing of complex components by electron beam melting. Materials Technology, 2009; 24: 180-190.

[14] Zhang L-C, Liu Y, Li S, Hao Y. Additive manufacturing of titanium alloys by electron beam melting: A review. Advanced Engineered Materials, 2018; 20 170084

[15] Galati M, Iuliano L. A literature review of powder-based electron beam melting focusing on numerical simulations. Additive Manufacturing, 2018; 19: 1–20

[16] Ding R, Guo ZX, Wilson A. Microstructural evolution of a Ti–6Al–4V alloy during thermomechanical processing. Materials Science and Engineering. 2002; A327: 233–245

[17] Fan Y, Tian W, Guo Y, Sun Z, Xu J. Relationships among the microstructure, mechanical properties, and fatigue behavior in thin Ti6Al4V. Advances in Materials Science and Engineering. 2016 http://dx.doi.org/10.1155/2016/7278267

[18] Vrancken B, Thijs L, Kruth JP, Van Humbeeck J. Heat treatment of Ti6Al4V produced by Selective Laser Melting: Microstructure and Mechanical properties. Journal of Alloys and Compounds, 2012; 541(0): 177-185.

[19] Pinke P, Réger M, Heat treatment of the Casted Ti6Al4V Titanium Alloy, Materials Science and Technology, Vol. 5, Special Issue– Constructional Materials 2005, Internet Journal, MTF S

[20] Crupi V, Epasto G, Guglielmino E, Squillace A. Influence of microstructure [alpha + beta and beta] on very high cycle fatigue behaviour of Ti-6Al-4V alloy. International Journal of Fatigue, 2017; 95: 64–75

[21] Benedetti M, Fontanari V. The effect of bi-modal and lamellar microstructures of Ti-6Al-4V on the behaviour of fatigue cracks emanating from edge-notches. Fatigue Fract Engng Mater Struct, 2004; 27: 1073–1089

[22] Svensson M, Ackelid U. Titanium alloys manufactured with electron beam melting mechanical and chemical properties. In: Proceedings of the Materials and Processes for Medical Devices Conference, 2010, p. 189-94

[23] Badea L, Surand M, Ruau J, Viguier B. Creep behavior of Ti-6Al-4V from 450° to 600°C. U.P.B. Sci., Series B, 2014; 76 (1): 185-196

[24] Koike J, Maruyama K. Study of primary creep in Ti-6-22-22S alloys. Materials Science and Engineering A, 1999; 263 (2): 155-159